Extremely Broadband Topological Surface States in a Photonic Topological Metamaterial

Minkyung Kim, Wenlong Gao, Dasol Lee, Taewoo Ha, Teun-Teun Kim, Shuang Zhang, and Junsuk Rho*

Metamaterials, artificially engineered materials consisting of subwavelength unit cells, have shown potentials in light manipulation with their extraordinary optical properties. Especially, photonic topological metamaterials possessing topologically protected surface states enable extremely robust control of light. Here, an extremely broadband topological phase in photonic topological metamaterials is demonstrated. In particular, topological surface states are observed for all the frequencies below a certain cut-off, originating from a double Weyl point at zero frequency. The extreme bandwidth and robustness of the photonic topological metamaterial are beneficial for practical applications such as one-way waveguide and photonic integrated systems but also advantageous in design and fabrication since the only necessary condition is to satisfy the effective hyperbolic and chiral properties, without entailing strict periodic arrangement.

1. Introduction

Recent discovery of Weyl fermion in certain crystals, which had been only previously predicted in quantum field theory,[1,2] have opened a new realm of condensed matter physics.[3] The photonic analogy of Weyl degeneracies has been soon implemented in photonics.[4–8] Besides Weyl points, other topological states, such as quantum Hall effect and quantum spin Hall effect have been also predicted and observed in photonics.[9–18] During the last

M. Kim, D. Lee, Prof. J. Rho
Department of Mechanical Engineering
Pohang University of Science and Technology (POSTECH)
Pohang 37673, Republic of Korea
E-mail: jsrho@postech.ac.kr
Dr. W. Gao, Prof. S. Zhang
School of Physics and Astronomy
University of Birmingham
Birmingham B15 2TT, UK
Dr. T. Ha, Dr. T.-T. Kim
Center for Integrated Nanostructure Physics (CINAP)
Institute for Basic Science (IBS)
Suwon 16419, Republic of Korea
Dr. T. Ha, Dr. T.-T. Kim
Sungkyunkwan University
Suwon 16419, Republic of Korea
Prof. J. Rho
Department of Chemical Engineering
Pohang University of Science and Technology (POSTECH)
Pohang 37673, Republic of Korea

The ORCID identification number(s) for the author(s) of this article
can be found under https://doi.org/10.1002/adom.201900900.

DOI: 10.1002/adom.201900900

several years, photonic topological systems have developed rapidly, revealing many exotic phenomena including photonic topological surface states, chiral anomalies, and Weyl degeneracies. Weyl points, monopoles of Berry curvature in the momentum space with integer topological charges, are manifestations of the photonic Weyl systems, which are endowed with topological surface states, or photonic Fermi arcs that connect Weyl points with the opposite topological charges.

In the field of topological photonics, most of the studies have been performed in the regime of photonic crystal where periodicity is comparable to the wavelength. There are also a few works based on metamaterials, artificially structured optical materials composed of unit cells much smaller than the wavelength.[4,5,19,20] The mechanism of the metamaterial-based approaches is fundamentally different from photonic crystal-based ones, relying on the combination of two distinct properties: hyperbolicity and chirality. Existence of topologically protected surface states and photonic Weyl points in a medium with hyperbolic and chiral responses have been theoretically predicted[4,19] and experimentally demonstrated[5] recently. Since the topological surface states are formed between the Weyl point pairs, bandwidth of the surface states is related to the frequencies of the Weyl points. Here, we present a photonic topological metamaterial with a double Weyl point at zero frequency, generating extremely broadband topological surface states. The zero frequency Weyl point sets the lower limit of the bandwidth, so that the topological surface states exist at all frequencies below a certain frequency carrying the other Weyl point pair. Focused on three lowest bands, there exist six pairs of Weyl points, among which two have multiple topological charges. Chern numbers directly calculated from the simulated eigenmodes and experimentally observed surface waves support our result. The presence of topological surface states across a very broad bandwidth may lead to potential applications in topologically protected integrated photonic circuits.

2. Results and Discussion

A typical hyperbolic metamaterial consists of an array of metallic wire embedded in a dielectric medium with deep subwavelength spacings.[21,22] This highly anisotropic geometry
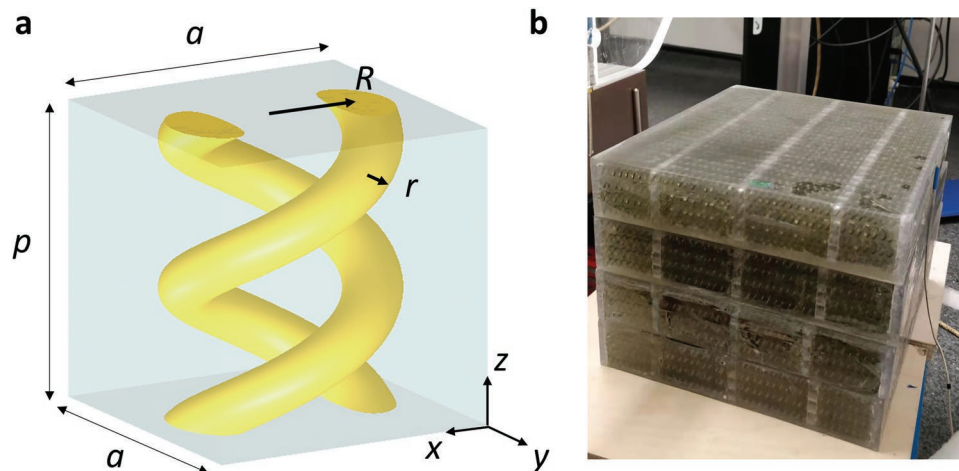
Figure 1. a) Two unit cells aligned along z-axis. The geometry parameters are given as: $a = 10$ mm, $p = 10$ mm, $R = 3$ mm, and $r = 1$ mm. b) Fabricated sample.

makes the wire system to have opposite signs of permittivity along the wires and perpendicular to the wires. However, straight wire array does not possess chirality due to the mirror symmetry. To simultaneously achieve hyperbolic properties and chirality in a single structure, we introduce long metallic helices.[23,24] One can expect that metallic helix structure has both hyperbolic and chiral properties, thereby possessing topologically nontrivial optical properties. Indeed, by adding a twist to the wire structure to break the inversion symmetry, the nodal line node is transformed into Weyl points.[25]

Two unit cells of the right-handed double-helix structure aligned along z-axis are illustrated in **Figure 1**a. Geometric parameters of the double-helix structure are set as the following: periodicity along x- and y-axis $a = 10$ mm, pitch $p = 10$ mm, helix radius $R = 3$ mm, and fiber radius $r = 1$ mm. Note that periodicity along z-axis is half of the pitch because the unit cell has screw symmetry; in other words, it is invariant under the $\pi/2$ rotation along z-axis followed by $p/4$ translation along z-axis. Considering the periodicity along z-axis, dispersion has C_4 symmetry along k_z-axis in a momentum space. Four blocks of sample are fabricated by embedding periodically arranged metallic springs in acrylic (Figure 1b). The unit cell is designed to work at microwave regime for the ease of fabrication and near-field imaging measurement, but by expanding or shrinking the size of unit cell, the topologically nontrivial system can operate at the higher frequencies (see Section S6 in the Supporting Information).

The retrieved effective parameters of the double-helix structure contain opposite signs of permittivity and nonzero chirality, satisfying both hyperbolic and chiral conditions (details can be found in Section S1 in the Supporting Information). We would like to note that while we employ periodically arranged structure to simulate band structures, effective hyperbolicity and chirality are the only necessary condition to achieve topological phase in the metamaterial regime, whereas lattice system with exact periodic arrangement is essential in photonic crystals.

In order to obtain band structure, we use eigenfrequency solver in COMSOL Multiphysics. For bulk states dispersion, a unit cell of real structure of metallic double-helix embedded in a dielectric is simulated with periodic boundary condition in all external boundaries. Perfect electric conductor condition is used

for metallic parts and refractive index of the surrounding dielectric medium is set as 2. Band structures and equifrequency curves of the double-helix structure are shown in **Figure 2**. Wave vectors are normalized by π/a for k_x and k_y and $2\pi/p$ for k_z. Here we focus on the lowest three bands. The bands have several point and line degeneracies which are presented as blue, yellow and red points and green lines. Circle and square points with the same color represent distinct point degeneracies forming a pair. Chern numbers are calculated based on Wilson loop method by using spatially averaged fields in the realistic structure instead of the effective Hamiltonian model (see Section S2 in the Supporting Information). The line degeneracy denoted as green line has no topological charge. On the other hand, the point degeneracies are all Weyl points with nonzero topological charges. Among them, the pair labeled as yellow circles is type 2 Weyl points and the others are type 1 Weyl points. Interestingly, two Weyl points, one at the Brillouin zone center (blue circle) and the other at the zone boundary (yellow square), are doubly charged and have partners of a pair of single charge of the opposite sign. The double or even multiple Weyl points have been predicted and reported in condensed matter physics[26–29] and also in photonics.[30,31] Whereas a Weyl point of single topological charge has a cone-shape dispersion near the Weyl point, the multiple Weyl points can either possess linear dispersion in all reciprocal directions[29] or have linear dispersion around the crossing point only in one reciprocal direction while exhibiting nonlinear dispersion along the other directions.[26,27] The double Weyl point denoted as blue circle has linear dispersion along k_z-axis. However, along k_x- and k_y-axes, one bulk state shows linear dispersion, whereas the other state has zero slope resulting from z-component of permittivity diverging to negative infinity (Figure 2a,b). Nonlinear and linear dispersion around the double Weyl point marked as yellow square can be found in Section S3 (Supporting Information). The doubly charged Weyl points are protected by C_4 and C_6 point group symmetries.[26] As such, by breaking the C_4 symmetry through designing different helix radius along x- and y-axis, the double Weyl point is split into two type 2 Weyl points with single charge (Section S4, Supporting Information).

Equifrequency curves at four frequencies and Chern numbers in each bulk state are shown in Figure 2c–f. Among
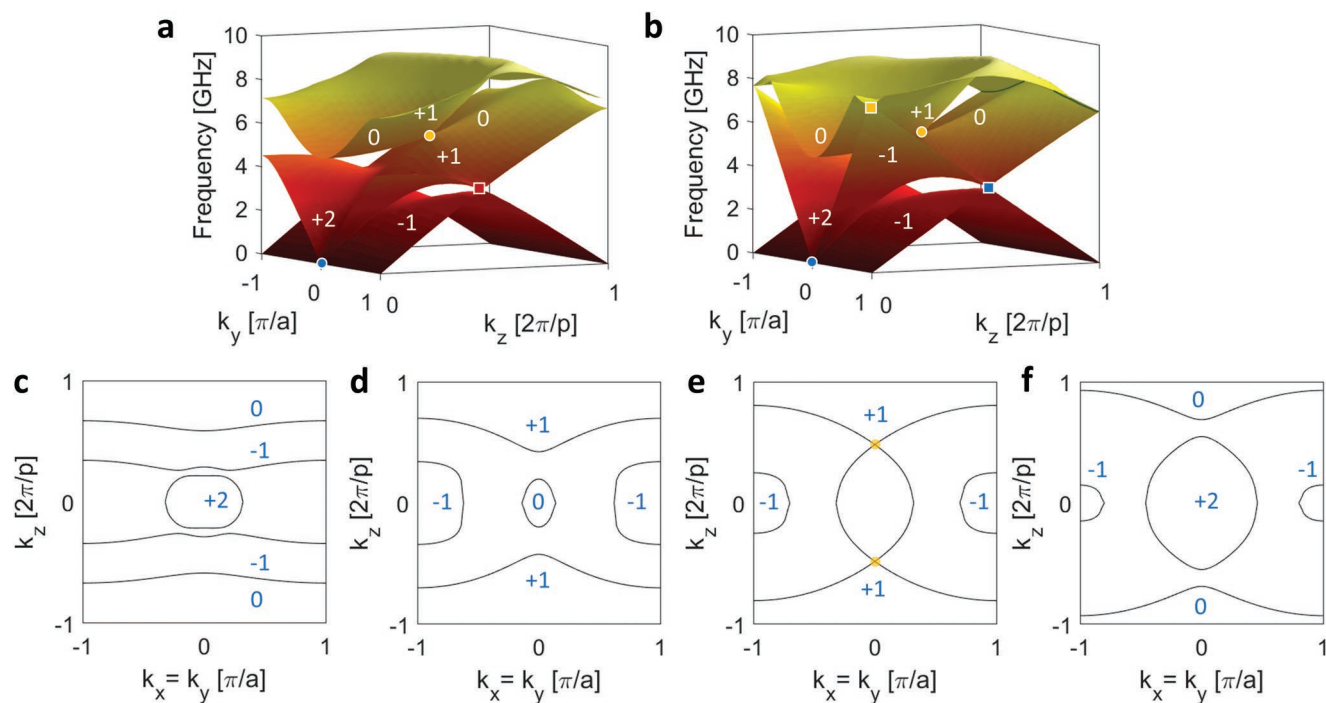
**ADVANCED
SCIENCE NEWS**

www.advancedsciencenews.com

**ADVANCED
OPTICAL
MATERIALS**

www.advopticalmat.de

Figure 2. Band structure of (a) $k_x = 0$ and (b) $k_x = k_y$ and Chern numbers. Equifrequency curves along a line $k_x = k_y$ and Chern numbers at (c) 2.5 GHz, (d) 5 GHz, (e) 5.71 GHz, and (f) 6.5 GHz. Circle and square points with the same color represent distinct Weyl points forming a pair.

six Weyl points, equifrequency curves at 5.71 GHz is shown (Figure 2e) because it is the only type 2 Weyl points. The Weyl points are marked as yellow circles, whose Chern number is calculated by non-Abelian Wilson loop method. In this time-invariant system, the sum of Chern numbers at a given frequency is zero, but each branch has different Chern number. According to the bulk-edge correspondence, topological surface states are expected between these momentum gaps between topologically inequivalent bulk states. Surface state dispersion is simulated by using supercell structure consisting of 19 unit cells aligned along x-axis, with boundary condition of perfect electric conductor, while the boundary conditions of the other directions are set to be periodic. Surface state dispersion at five different k_z are shown in **Figure 3**a–e. Between the first and the second bands, there exist topological surface states connecting the blue circle and square points. As one Weyl point is located at origin ($f = 0$) and the other point at 3.70 GHz, the double-helix structure supports topological surface states at all frequencies below 3.70 GHz. As opposed to previously reported topological surface states which have both lower and upper frequency limit, the surface states observed in the double-helix structure has no lower limit and are hence extremely broadband. Also, the surface states connected to the zero frequency Weyl point appear as a pair due to the double charge of the Weyl point. The another states not shown in Figure 3a–e can be found by converting k_z to $-k_z$ (Figure 3f). Other surface states connecting the red circle and square points are also found. Here, the surface states connecting the Weyl point pair marked as red points only appear in narrow bandwidth near 3.66 GHz where the point degeneracies are located. Figure 3 also shows the existence of topological surface states between the second and the third bands. When $|k_z|$ is larger than 0.48 within which all Weyl points are located,

the surface states disappear due to the neutralized topological charges.

Electric field distributions in logarithmic scale of two counter-propagating surface state at 3 GHz are shown in Figure 3g,h. Gradient of electric field amplitude indicates highly localized surface waves at each side. If the surface states are indeed topologically protected, their propagation should be extremely robust against perturbations such as defects and cannot be backscattered. To confirm this topological property, surface waves propagating along the sharp edge are shown in Figure 3i. Since the double-helix structure is working in a metamaterial regime where unit cell is much smaller than the wavelength, homogeneous medium with the retrieved effective parameter (shown in Section S1, Supporting Information) is used instead of the real structure. Line current excites specific k_z between the topologically nontrivial bandgap, generating robust surface waves which are not scattered by an arbitrarily shaped obstacle. Although we only focus on the surface states between three lowest bands, surface states connecting the higher bands are also observed (shown in Figure 3f), indicating the double-helix structure also works in photonic crystal regime.

Finally, we experimentally demonstrate the existence of topologically protected surface states in a broad frequency range. y-polarized source placed near the one side of sample excites the surface waves and y-component of electric fields propagating on the surface of fabricated sample are measured by near-field scanning setup. The experiments are performed in two schemes. Surface waves on the top surface of the 2 by 2 stacked layers at 4.4 GHz shows the one-way propagating surface waves (**Figure 4**a). To demonstrate the backscattering immune propagation along sharp edges, we use the similar experimental setup shown in Figure 3i. In this step-like measurement setup, the surface state is further confirmed by scanning both top and
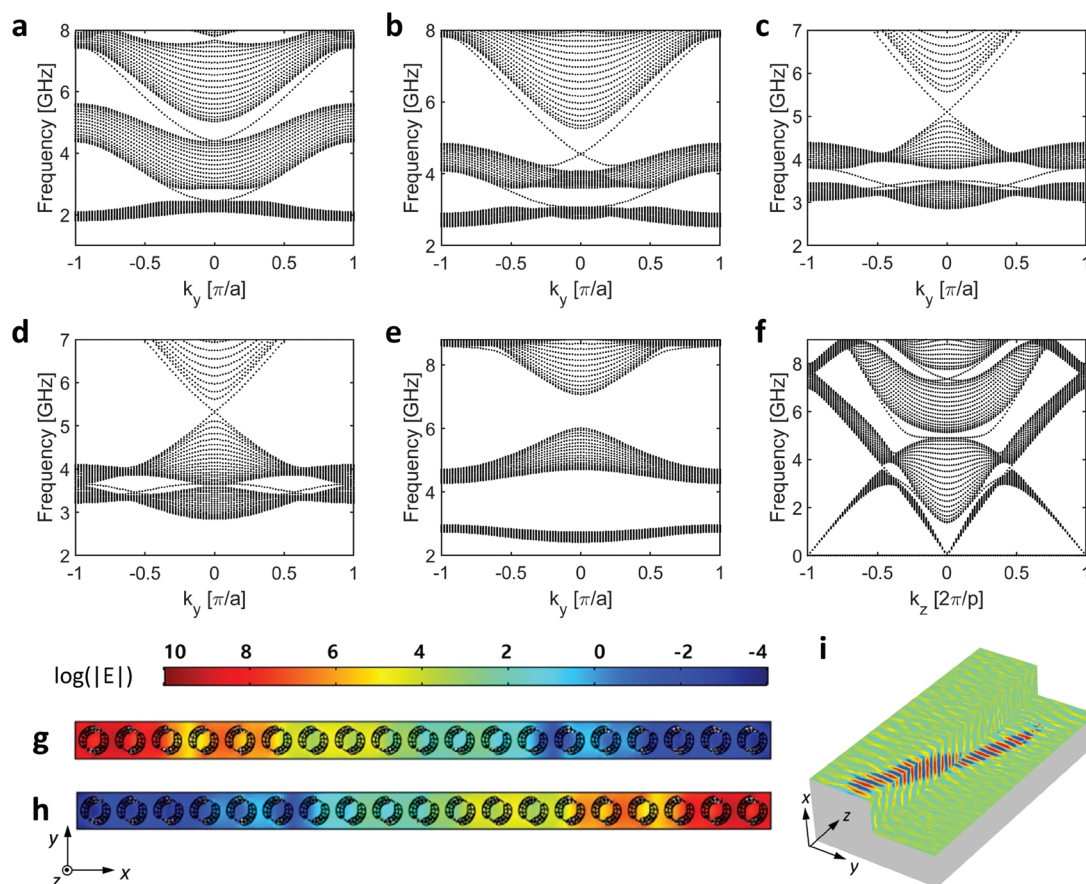
Figure 3. Band structures with surface states when $k_x = 0$ and (a) $k_z = 0.25$, (b) $k_z = 0.35$, (c) $k_z = 0.42$, (d) $k_z = 0.45$, (e) $k_z = 0.6$, and (f) $k_y = 0.25$. Electric field amplitude in logarithmic scale of surface state at 3 GHz when $k_x = 0$, $k_y = 0.25$, (g) $k_z = 0.317$, and (h) $k_z = -0.317$. i) x-component of electric field of surface waves at 3 GHz.
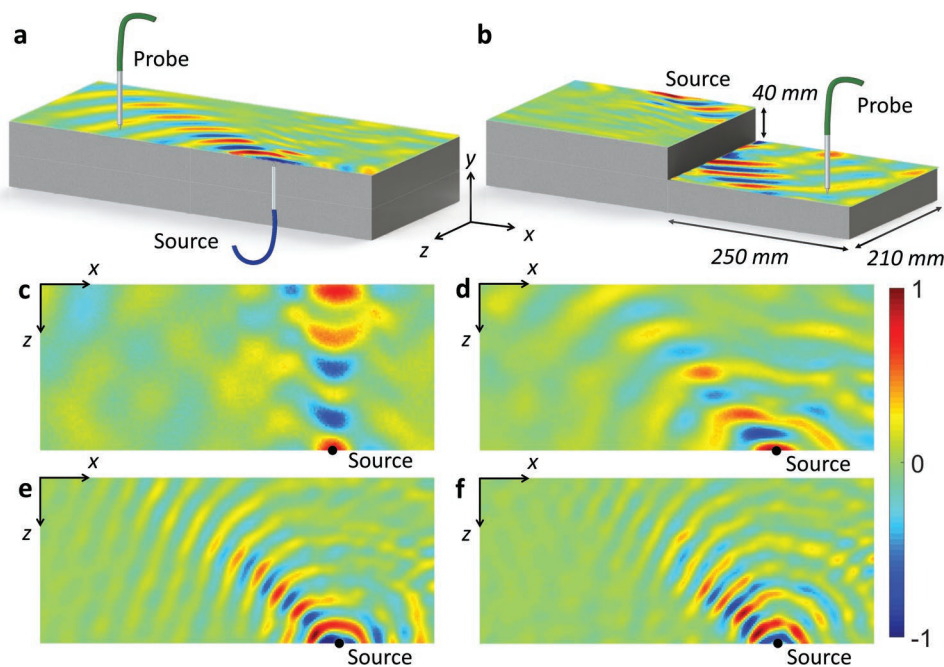

Figure 4. a,b) Near-field scanning experimental setup with experimentally measured instantaneous electric field at 4.4 GHz for (a) stacked layer and (b) step-like sample. c–f) Electric field experimentally measured by the stacked layer setup at (c) 1.7 GHz, (d) 3.8 GHz, (e) 8.3 GHz, and (f) 9.0 GHz. The source and the probe are y-polarized.

the bottom surface while exciting the surface waves at the top surface (Figure 4b). The one-way propagating surface states are also experimentally observed in a broadband range including 1.7, 3.8, 8.3, and 9.0 GHz (Figure 4c–f). We would like to note that since the dielectric part of the fabricated sample is acrylic, which has lower refractive index compared to the index used for numerical simulation, working frequency is blueshifted. However, the use of dielectric with lower refractive index only affects the frequency of the Weyl points while keeping the main features such as existence of the Weyl points and the topological properties (Section S5, Supporting Information).

3. Conclusion

In conclusion, double Weyl points and extremely broadband topological surface states residing in a double-helix structure are presented. Unlike topological photonic crystals, this topological metamaterial relies on effective hyperbolicity and chirality, which forces a Weyl point with double topological charge in zero frequency. We observe six pairs of Weyl points and broadband topological surface states connecting them, which are robust against deformation. The extreme broad bandwidth and robustness will be beneficial for applications such as one-way waveguide and photonic integrated circuits.

4. Experimental Section

Fabrication: Four blocks of samples (250 mm × 210 mm × 40 mm) were fabricated by 3D fabrication company (3Dmakers). Each block of sample contained 25 × 4 periods of double helices (made of JIS G3522) embedded in acrylic, and each helix had 25 turns.

Measurement: For near-field scanning measurement, 2 by 2 stacked layers were excited by *y*-polarized source and the surface waves on the top surface were detected by *y*-polarized probe. A step-like geometry was made by stacking two blocks of sample on one side and placing one block on the other side. Both the top and bottom surfaces of the step-like sample were scanned, while exciting the top surface.

Supporting Information

Supporting Information is available from the Wiley Online Library or from the author.

Conflict of Interest

The authors declare no conflict of interest.

[1] H. Weyl, *Z. Phys.* **1929**, *56*, 330.
[2] L. Balents, *Physics* **2011**, *4*, 36.
[3] S.-Y. Xu, I. Belopolski, N. Alidoust, M. Neupane, G. Bian, C. Zhang, R. Sankar, G. Chang, Z. Yuan, C.-C. Lee, S.-M. Huang, H. Zheng, J. Ma, D. S. Sanchez, B. Wang, A. Bansil, F. Chou, P. P. Shibayev, H. Lin, S. Jia, M. Z. Hasan, *Science* **2015**, *349*, 613.
[4] M. Xiao, Q. Lin, S. Fan, *Phys. Rev. Lett.* **2016**, *117*, 057401.
[5] B. Yang, Q. Guo, B. Tremain, L. E. Barr, W. Gao, H. Liu, B. Béri, Y. Xiang, D. Fan, A. P. Hibbins, S. Zhang, *Nat. Commun.* **2017**, *8*, 97.
[6] L. Lu, L. Fu, J. D. Joannopoulos, M. Soljačić, *Nat. Photonics* **2013**, *7*, 294.
[7] J. Noh, S. Huang, D. Leykam, Y. D. Chong, K. P. Chen, M. C. Rechtsman, *Nat. Phys.* **2017**, *13*, 611.
[8] B. Yang, Q. Guo, B. Tremain, R. Liu, L. E. Barr, Q. Yan, W. Gao, H. Liu, Y. Xiang, J. Chen, C. Fang, A. Hibbins, L. Lu, S. Zhang, *Science* **2018**, *359*, 1013.
[9] F. D. M. Haldane, S. Raghu, *Phys. Rev. Lett.* **2008**, *100*, 013904.
[10] S. Raghu, F. D. M. Haldane, *Phys. Rev. A* **2008**, *78*, 033834.
[11] Z. Wang, Y. D. Chong, J. D. Joannopoulos, M. Soljačić, *Phys. Rev. Lett.* **2008**, *100*, 013905.
[12] Z. Wang, Y. Chong, J. D. Joannopoulos, M. Soljačić, *Nature* **2009**, *461*, 772.
[13] M. Hafezi, E. A. Demler, M. D. Lukin, J. M. Taylor, *Nat. Phys.* **2011**, *7*, 907.
[14] K. Fang, Z. Yu, S. Fan, *Nat. Photonics* **2012**, *6*, 782.
[15] A. B. Khanikaev, S. H. Mousavi, W.-K. Tse, M. Kargarian, A. H. MacDonald, G. Shvets, *Nat. Mater.* **2013**, *12*, 233.
[16] S. A. Skirlo, L. Lu, M. Soljačić, *Phys. Rev. Lett.* **2014**, *113*, 113904.
[17] M. Hafezi, S. Mittal, J. Fan, A. Migdall, J. M. Taylor, *Nat. Photonics* **2013**, *7*, 1001.
[18] M. C. Rechtsman, J. M. Zeuner, Y. Plotnik, Y. Lumer, D. Podolsky, F. Dreisow, S. Nolte, M. Segev, A. Szameit, *Nature* **2013**, *496*, 196.
[19] W. Gao, M. Lawrence, B. Yang, F. Liu, F. Fang, B. Béri, J. Li, S. Zhang, *Phys. Rev. Lett.* **2015**, *114*, 037402.
[20] M. Kim, D. Lee, D. Lee, J. Rho, *Phys. Rev. B* **2019**, *99*, 235423.
[21] P. A. Belov, R. Marqués, S. I. Maslovski, I. S. Nefedov, M. Silveirinha, C. R. Simovski, S. A. Tretyakov, *Phys. Rev. B* **2003**, *67*, 113103.
[22] A. Poddubny, I. Iorsh, P. Belov, Y. Kivshar, *Nat. Photonics* **2013**, *7*, 948.
[23] J. K. Gansel, M. Thiel, M. S. Rill, M. Decker, K. Bade, V. Saile, G. von Freymann, S. Linden, M. Wegener, *Science* **2009**, *325*, 1513.
[24] J. K. Gansel, M. Wegener, S. Burger, S. Linden, *Opt. Express* **2010**, *18*, 1059.
[25] L. Lu, J. D. Joannopoulos, M. Soljačić, *Nat. Photonics* **2014**, *8*, 821.
[26] C. Fang, M. J. Gilbert, X. Dai, B. A. Bernevig, *Phys. Rev. Lett.* **2012**, *108*, 266802.
[27] S.-K. Jian, H. Yao, *Phys. Rev. B* **2015**, *92*, 045121.
[28] S.-M. Huang, S.-Y. Xu, I. Belopolski, C.-C. Lee, G. Chang, T.-R. Chang, B. Wang, N. Alidoust, G. Bian, M. Neupane, D. Sanchez, H. Zheng, H.-T. Jeng, A. Bansil, T. Neupert, H. Lin, M. Z. Hasan, *Proc. Natl. Acad. Sci. USA* **2016**, *113*, 1180.
[29] T. Zhang, Z. Song, A. Alexandradinata, H. Weng, C. Fang, L. Lu, Z. Fang, *Phys. Rev. Lett.* **2018**, *120*, 016401.
[30] W.-J. Chen, M. Xiao, C. T. Chan, *Nat. Commun.* **2016**, *7*, 13038.
[31] M.-L. Chang, M. Xiao, W.-J. Chen, C. T. Chan, *Phys. Rev. B* **2017**, *95*, 125136.